The Meteoritical Society

Meteoritics & Planetary Science 42, Nr 4/5, 883–894 (2007)
Abstract available online at http://meteoritics.org

Possible reasons of shock melt deficiency in the Bosumtwi drill cores

N. ARTEMIEVA

Institute for Dynamics of Geospheres, Leninsky Prospect 38, Building 1, 119334, Moscow, Russia
Planetary Science Institute, 1700 East Fort Lowell, Tucson, Arizona 85719, USA
E-mail: artemeva@psi.edu

(Received 30 October 2006; revision accepted 17 January 2007)

Abstract–Pre-drilling numerical modeling of the Bosumtwi impact event predicted a 200 m thick coherent melt layer, as well as abundant highly shocked target material within the central part of the crater structure. However, these predictions are in disagreement with data from drill core obtained in 2004–2005. Here I provide a brief overview of previous results and discuss possible reasons behind melt deficiency, such as specific impact scenarios (low impact velocity and/or low impact angle), and specific target properties (different composition, high porosity, high content of volatiles). I conclude that the most likely explanation is the dispersion of impactites due to the vaporization of pore water, which was not included in the original numerical model.

INTRODUCTION

Numerical modeling of the Bosumtwi impact event (Artemieva et al. 2004) was published just a few months before the International Continental Scientific Drilling Program (ICDP) drilling project began (Koeberl et al. 2005). This work showed encouraging correlations between the model and observations: the calculated crater size and its shape were comparable with the Bosumtwi crater geometry (Scholz et al. 2002; Karp et al. 2002); the distribution of tektites and microtektites was validated against the Ivory Coast strewn field study (Glass et al. 1991); and predictions of melt volume within the crater were comparable to the magnetic model by Plado et al. (2000). We also hoped that our numerical study would provide valid predictions of the physical properties of the rocks in the drill cores: the value of maximum shock compression could be directly connected with shock metamorphic features in the target rocks; the presence of projectile material could be confirmed by geochemical analysis of brecciated materials and melts; the temperature distribution would constrain the region of natural remanent magnetization and, in combination with predicted fracture distribution, would define the zone of intensive post-impact hydrothermal activity. However, the available core material is substantially different from our predictions. The most surprising features are: 1) a total absence of a coherent melt sheet and a very low melt or diaplectic glass content in core suevite (Coney et al. 2007; Deutsch et al. 2007; Morrow 2007), and 2) the high porosity of the impactites and their strong inherent mixing, i.e., the absence of any trends in shock metamorphism of clasts with depth (Koeberl et al. 2005; Deutsch et al. 2006; Reimold et al. 2006). Only a minor decrease of the abundance of shocked quartz grains as well as the number of PDFs per grain has been found in the brecciated bedrock with increasing depth (Ferrière et al. 2007; Deutsch et al. 2007).

In the first part of this paper, I provide a brief overview of pre-drilling assumptions, applied numerical methods, and the obtained results (a summary of Artemieva et al. 2004). Then I discuss possible reasons for the discrepancies between the model predictions and drill core observations and data.

PRE-DRILLING MELT ESTIMATES

Geological and Geophysical Survey

Melt is a common feature in the Earth's impact craters formed in crystalline target rocks (Grieve and Cintala 1992). Geological field studies of impact melt occurrences is often complicated by poor crater preservation on Earth, and an absence of intensive deep drilling in large craters. As significant melting and vaporization do not occur in impacts at velocities currently achievable in the laboratory, a detailed study of the production of melt and vapor in planetary impact events can only be carried out using hydrocode simulations (Ahrens and O'Keefe 1977; Pierazzo et al. 1997; Ivanov and Artemieva 2002). A comparison of numerical results with structural geological and geophysical data provides a test of the model assumptions and crater size estimates.

© The Meteoritical Society, 2007. Printed in USA.

The increase of melt volume with increasing crater diameter is a well-known trend (see Fig. 3 in Grieve and Cintala 1992). Exceptions occur for craters formed in sedimentary targets or with substantial sedimentary supracrustal target component (e.g., Meteor Crater, Logoisk, Ries). The craters with diameters similar to that of the Bosumtwi, from the database by Grieve and Cintala (1992), are Ilyinets (8 km in diameter) and Kaluga (15 km) with 0.7 and 8 km^3 of impact melt, respectively. The Bosumtwi crater is also associated with the Ivory Coast tektite strewn field (Koeberl et al. 1998, and references therein), an expansive region of distal, molten ejecta deposited to the SW of Bosumtwi. In 1997 a high-resolution airborne geophysical survey revealed a halo-shaped magnetic anomaly in the area of the Bosumtwi crater (Pesonen et al. 1998; Plado et al. 2000). It was presumed that a <400 m thick magnetic lens of ~2.2 km^3 (i.e., at least 2.6 km in diameter) normally magnetized material, consisting of impact-melt breccias, produces this magnetic anomaly.

Numerical Model and Results

In Artemieva et al. (2004), two well-tested and widely applied impact hydrocodes, SOVA (Shuvalov et al. 1999) and SALE (Amsden et al. 1980), were used to model the Bosumtwi crater formation. We assumed that the target consisted of a homogeneous crystalline layer, modeled with the ANEOS equation of state for granite (Pierazzo et al. 1997); the target was in hydrostatic equilibrium and had a temperature gradient of 13 °C/km, corresponding to the "cold" spot of the Earth's crust (80 °C at a depth of 6 km). The projectile was modeled with the same EOS, but treated in the hydrocode as a separate material, with an accurate definition of target-projectile boundaries.

Tracer Technique

Both SALEB and SOVA employ an Eulerian coordinate system; thus, tracer particles must be used to record the thermodynamic history (density, pressure, temperature) of any given "parcel" of material as it moves through the mesh. The tracers are massless particles (and hence have no effect on the flow field) that move with local velocity at the current tracer position. The thermodynamic history of the tracer can be used to establish the degree to which the material represented by the tracer has undergone melting and vaporization. This technique is widely used to determine the total volumes of melt and vapor produced during the impact (Pierazzo et al. 1997; Pierazzo and Melosh 2000; Ivanov and Artemieva 2002), by recording the maximum entropy (or pressure) reached by the tracer in shock compression (Zel'dovich and Raizer 2002; Ahrens and O'Keefe 1972). As decompression is an isentropic process, the total melt or vapor volume may be defined by summing up the volume of material represented by tracers with an entropy value higher than that required for melting-vaporization under standard conditions (i.e., atmospheric pressure), readily found in the literature (Pierazzo et al. 1997). The alternative approach for calculating final melt volumes is to run the impact simulation until the final crater has been formed and compare the final cell-centered pressure-temperature distributions with the corresponding solidus-liquidus of geological materials.

Both methods for melt-volume estimation, the tracer particle method and the direct method, have errors associated with them. In the tracer particle method, the maximum entropy is reached on the shock front in a very narrow zone and, hence, depends, undesirably, on the computational method and artificial viscosity, the rheological model, and, strongly, on the mesh resolution. Also not all materials are unloaded to standard pressure, especially in large craters. A comparison with geological observations leads to additional complications when the tracer-particle method is used. First, solid material density is usually higher than melt density, i.e., real melt volume is equal to the sum of tracer volumes multiplied by the ratio of these densities of ~1.1. Second, part of the impact melt is ejected from the crater and may be found outside the rim in a mixture with lithic fragments (as a suevite) or as pure melt—tektites and microtektites. The percentage of ejected material depends on the chosen impact scenario and could reach 30–50%. On the other hand, part of hot rocks from the crater walls could be digested by overheated shock melt increasing visible "melt" volumes up to 30% (Simonds and Kieffer 1993). The direct method allows these problems to be partially taken into account. The direct method has the drawback that at the end of the calculation a lot of computational cells contain a mixture of molten and non-molten materials with an average temperature below that required for melting. Also energy losses and advective diffusion (unavoidable in Eulerian methods) during the long-term calculations tend to decrease final temperatures. The ideal solution is a combination of both methods on an extremely fine computational grid; however, in general, this procedure is computationally too expensive. The tracer-particle method has the distinct advantage that it does not require long-term computation until the final crater is formed to measure the melt volume, and is thus the typical method of choice.

Melt Volume

The numerical models of Pierazzo et al. (1997) showed that the ratio of the melt volume V_m to the projectile volume V_{pr} is related to the impact velocity U by the equation $\log(V_m/V_{pr}) = a + 3/2\mu \log(U^2/E_m)$, with the coefficients $a = -0.595 \pm 0.064$, $\mu = 0.667 \pm 0.017$, and melting energy $E_m = 5.2 \times 10^6$ J/kg. For a 20 km/s vertical impact this means that $V_m = (15 \div 25)\ V_{pr}$, which for estimates of the Bosumtwi projectile volume give $V_m = 2.6$–4.3 km^3. A comparison of the calculated melt volumes with estimates of actual melt volumes from the database of terrestrial craters (Grieve and

Cintala 1992), shows good agreement with observational estimates, although there is a systematic trend that the numerical results are higher than observational estimates. In Artemieva et al. (2004), calculations of the Bosumtwi melt volume (including vapor) after a vertical impact varied from 2.3 km^3 (asteroid impact with minimum velocity of 11 km/s) to 8.7 km^3 (cometary impact with velocity of 40 km/s). An oblique impact creates additional uncertainty, because the effect of impact angle on melt production and final crater diameter has not been fully quantified (Pierazzo and Melosh 2000; Ivanov and Artemieva 2002). In Artemieva et al. (2004) we considered two endmember cases where either (1) the crater size for a natural impact scales with impact angle in the same manner as for laboratory impacts (Chapman and McKinnon 1986) and, hence, the projectile size necessary to form the Bosumtwi crater increases as impact angle decreases (i.e., crater diameter scales with $\sin \theta^{-0.57}$); or (2) a high-velocity oblique impact has almost the same efficiency as a vertical one from the viewpoint of crater volume (Ivanov and Artemieva 2002). In the latter case the projectile size does not depend on the impact angle or at least depends much more weakly than $\sin \theta^{-0.57}$ (this assumption is certainly only valid in a restricted range of the impact angles, as a grazing impact does not create any melt or crater). Absolute melt volumes determined for these two endmember cases are shown in Table 1 (volumes using the scaling of Chapman and McKinnon [1986] are in bold). Previous numerical investigations of tektite formation, transport, and deposition suggest that the impact angle for the Bosumtwi crater event was in the range of 30–45° (Artemieva 2002) and impact velocity of about 20 km/s; thus, the most probable value of the total melt was predicted as 2.6–3.9 km^3 (Table 1).

Thickness of the Melt Sheet

Not all the melt is deposited inside the crater. In a vertical and especially in an oblique impact, a substantial part is ejected from the crater with high velocity to form distal ejecta (tektites and microtektites), or with lower velocity in a mixture with fine solid ejecta and later deposits inside or in the vicinity of the crater (suevite). For a vertical impact with a velocity of 15 km/s, only 68% of the total melt (or 2.2 km^3) may be found within the crater as a homogeneous impact-melt sheet and as a mixture of solid and molten material, suevite (Artemieva et al. 2004). According to the model, all the melt retained in the crater is located in the central part of the crater, with a thickness of about 200 m at distances up to 1.5 km from the crater's center (melt pool). At larger distances the thickness of the melt sheet drops abruptly to 20–30 m implying that this melt is probably mixed with solid material (Fig. 1). These estimates are consistent with melt volume estimates based on the magnetic model by Plado et al. (2000) and petrographic observations at other impact structures (e.g., Lappäjarvi, W. U. Reimold, personal communication). After an oblique impact at 30–45° with a velocity of 15 km/s the melt volume inside the crater is in the range of 65–70% of the total melt, depending on the impact angle. In this case, the thickness of the melt sheet should be essentially the same as after a vertical impact, as the late stage of crater formation (including crater collapse and melt spreading) is quasi-symmetric, although the complete crater formation process was not modeled for oblique impacts.

Table 1. Melt production (in km^3) versus impact velocity and impact angle. Numbers in bold are for the projectile scaling with impact obliquity (see text for details)

Impact velocity (km/s)	Impact angle				
	90°	60°	45°	30°	15°
40 (comet)	8.7	7.9	6.5	3.7	1.0
	8.7	**9.9**	**11.6**	**12.1**	**9.8**
20	4.7	4.5	3.9	2.6	0.6
	4.7	**5.8**	**7.2**	**8.6**	**6.1**
15	3.2	–	2.6	1.6	–
	3.2	**–**	**4.6**	**5.3**	–
11.2	2.3	2.0	1.6	0.8	–
	2.3	**2.6**	**2.8**	**2.4**	–

Shock Metamorphism in the Rocks

The tracer particle technique allows peak shock pressure profiles with depth to be constructed at certain distances from the crater center (see Fig. 2). In the central column, the material is subjected to the highest compression at the initial stage of the impact and is displaced only vertically (this is the result of vertical impact and axial symmetry). At this location, the final thickness of the target material with a high degree of shock metamorphism (37–10 GPa) is about 2 km. In contrast, the column 2.5 km from the center of the final crater is subjected to less compression during the impact; the material with a high degree of compression is deposited there because of radial spreading from the crater's center. Thus, its thickness is less than 200 m (at the depth of 0.8 to 1 km) with a sharp decrease to weakly shocked materials (maximum compression less than 5 GPa).

POSSIBLE REASONS BEHIND LOW MELT CONTENT IN DRILL CORES

Our predictions have not been confirmed by the drilling results. Neither of the deep cores, LB-07A and LB-08A (their positions are shown in Fig. 1), intersected a coherent melt sheet; the thickness of the suevite layer in LB-07A is less than 50 m (Reimold et al. 2006; Coney et al. 2007), while in LB-08A it occurs as fallback suevite in the upper 20 m and deeper exclusively in dikes (Deutsch et al. 2006; Deutsch et al. 2007; Ferrière et al. 2007). In this section I discuss potential explanations for the discrepancy between the numerical and geophysical model predictions and the observational results.

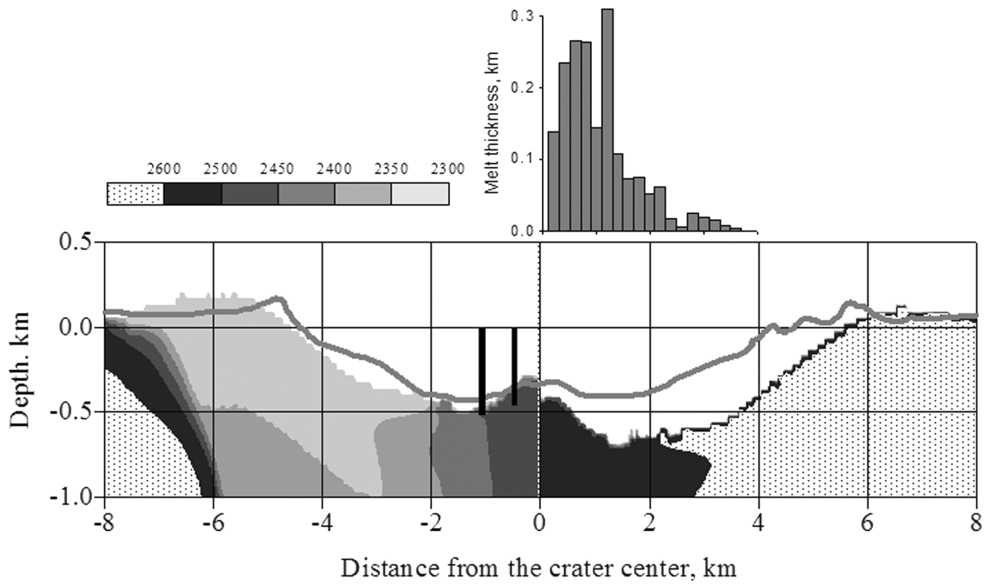

Fig. 1. Density distribution in target rocks as reproduced by the SALE numerical model (on the right) and with additional bulking (on the left) in comparison with real crater topography (thick gray line). Vertical black lines marks an approximate position of the drill cores. The top panel shows calculated thickness of the melt sheet after vertical impact at 15 km/s projectile velocity (modified after Artemieva et al. 2004).

Do the Two Cores Adequately Represent the Bosumtwi Impact Structure?

All drilling operations took place on good-quality seismic lines (Scholz et al. 2002; Karp et al. 2002). The borehole LB-07A was drilled in the deep crater moat to a depth of 540 m, whereas the LB-08A core was drilled on the outer flank of the central uplift to a depth of 450 m, as these features were identified in seismic profiles. The base of post-impact sediments (apparent depth of a fresh crater) occurred at the depths of 333 and 235 m, respectively. Drilling progressed in both cases through the assumed melt rock/impact breccia layer into fractured bedrock.

Have the boreholes reached the true depth of the crater or have they stopped erroneously at a large block of fractured rocks slumping from the crater walls? Is it possible that the real melt pool is below this level? Based on the measurements at complex terrestrial impact structures (Grieve and Robertson 1979; Grieve and Pesonen 1992), the value of true crater depth H_T for Bosumtwi is 0.82 km (using $H_T = 0.52D^{0.2}$, where D = 10.5 km is the rim-to-rim crater diameter), whereas the value of apparent crater depth should be 0.41 km ($H_A = 0.15D^{0.43}$). These approximations have been obtained for craters in the range 10 to 100 km, but are not absolutely reliable, as data scattering is quite large because of erosion effects. The difference between these depths corresponds to the total thickness of impactites (maximum depth of allochthonous breccia lens), which for Bosumtwi is: H_T-H_A = 400 m. This simple analysis suggests that the real apparent depth and especially the thickness of impactites in the Bosumtwi drill cores appear to be too small. However, the apparent crater depth (the top of breccia lens) is in good agreement with the seismic reconstruction of the Lake Bosumtwi structure (Scholz et al. 2002; Karp et al. 2002): a sharp change in sound speed velocity from 1.6 km/s (post-impact unconsolidated sediments) to 3.0 km/s (brecciated rocks) was found at the depth of 250–350 m in the central part of the crater. Below this level the sound speed increases gradually and complicates correct interpretation of the true crater depth. Numerical crater modeling (Fig. 3 of Artemieva et al. 2004) predicted a substantially deeper crater for all sets of rheological parameters. A simplified model for bulking allowed better consistency between topographic data and numerical model (Fig. 10 of Artemieva et al. 2004). But neither numerical model nor seismic reconstruction provide an absolute definition of the real crater depth and, thus, failed to confirm the correct maximum depth for drilling (the true crater floor).

The same models do not predict a melt pool below brecciated rocks, but consistently on their top. The situation of the true melt pool below the brecciated rocks occurs in small simple craters. Classic example is the well-studied and drilled 3.4 km diameter Brent crater in Canada (Grieve et al. 1977; Melosh 1989, p.127). Whereas the total melt volume is in a good agreement with the melt scaling relation, the melt rocks are not uniformly distributed throughout the breccia: a small, nearly homogeneous pool of solidified melt occurs near the base of the breccia lens, consisting of weakly shocked and homogeneous rocks; a more solidified melt occurs near the top of the breccia lens where it is mixed with an abundance of clasts from the bedrocks, showing a wide range of shock levels. At first glance, the situation with the Bosumtwi cores could be very similar, leading to the assumption that both cores may not have reached the melt pool.

However, the situation with larger complex craters is different and more complicated, as they are subjected to much more intensive modification during the collapse phase (Melosh 1989). The impactites' properties in the drill cores depend on the position of drilling (those within the central uplift show more regular structure) and target properties (a coherent melt sheet may be found within the craters in crystalline rocks, but rarely within the craters in sedimentary rocks or with thick sedimentary cover). A few craters on the territory of the former USSR, which have been intensively drilled, give us some interesting examples. The 25 km diameter Boltysh impact crater was formed in Precambrian granites and granite gneisses of the Ukrainian Shield (Gurov and Gurova 1985). The crater's deposits have undergone minimal post-impact erosion; two boreholes allow to study a complete vertical section of impactites within the annular trough, consisting of 20 m thick suevite and an about 200 m thick melt sheet (Grieve et al. 1987). Beneath the melt sheet the degree of shock induced deformation decreases rapidly, so that planar deformation features are absent ~150 m below the crater floor and the basement rocks are mostly fresh and only slightly fractured. The 15 km diameter Logoisk crater was formed in a mixed target with 200–300 m thick sedimentary sequence. Twenty eight boreholes were drilled within the crater. The true crater depth (authogenic breccia) was found at the depth of ~500–550 m in the central part of the crater; 200 m thick allogenic breccia containing tens of meters thick lenses of suevite with 10–60% of impact glass and PDFs in quartz clasts. Samples from the 5 km deep drill hole within the central uplift of the 80 km diameter Puchezh-Katunki impact crater (2 km thick sediments overlying crystalline basement in the pre-impact target) shows gradual changes in shock metamorphic features from 45 GPa (with some melt inclusions) near the surface to 10–15 GPa at the depth of 5 km (Pevzner et al. 1992; Ivanov 2002). In contrast to Boltysh, no coherent impact melt sheet was found in the annual trough, which is filled by allogenic breccia overlain by a thin suevite layer. Impactites from the 100 km diameter Popigai crater, formed in crystalline basement covered by 600 m thick sediments in Late Eocene, are distributed over an area of 5000 km^2. The crater was intensively studied and drilled because of its famous diamonds (Masaitis 1992; 1998). Diamond-bearing impact melt rocks and suevites in the Popigai crater interior occur as extended lens-like and sheet-like bodies, but also as irregular and small bodies. Impact melt sheets have a complex inner structure: separate horizontal layers are distinguished by degree of crystallinity and fragment abundance.

Two other well-known examples are the 24 km diameter Ries crater in Germany and the 180 km diameter Chicxulub structure in Mexico. The ratios of sediment thickness to the transient crater diameter are similar for these craters (~0.05 and ~0.03, respectively). The 1200 m deep drill core Nördlingen 1973 (Pohl et al. 1977) obtained 3.5 km from the Ries center revealed a 270 m thick suevitic layer underlain by an 80 m thick layer of megabreccia (fragments up to a few meters), and reached authogenic breccia at the depth of ~600 m. Only two occurrences of impact melt rock, with lateral extents of 10–50 m were found within the Ries crater in the megablock zone. Descriptions of the Chicxulub drill cores are summarized in Stöffler et al. (2004). Melt rocks have been found in a few drill cores (C1, S1, Y6) inside the central basin, but not within the Yax-1 borehole, where the suevite thickness is surprisingly (~100 m) low.

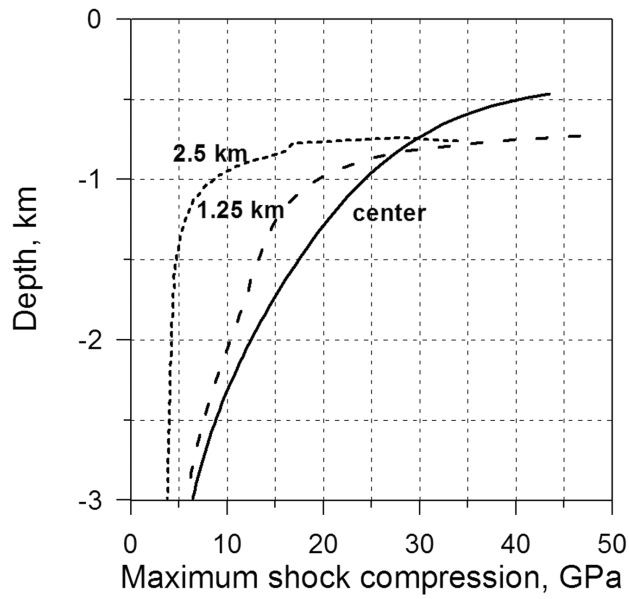

Fig. 2. Model results of maximum pressure versus depth for three potential Bosumtwi drill cores. The solid line is for the core in the crater center; the dashed and dotted lines are for cores at distances of 1.25 and 2.5 km from the center (modified after Artemieva et al. 2004).

Another unresolved problem is whether or not an impactite sequence of a crater in the tens of km size range can be robustly represented by a couple of cores a few cm in diameter each. In other words, what is the scale of nonhomogeneities in impact craters? This question demands expensive drilling programs and intensive high-resolution modeling in nonhomogeneous targets. The few mentioned examples show that impactite sequences within complex craters formed in mixed targets may be highly heterogeneous. In principle, the possibility of incorrect interpretation of obtained drill cores cannot be totally excluded on the basis of our present knowledge. However, the existing data provide the motivation to check the numerical model and to find its possible flaws.

Specific Impact Scenario

Low-velocity or low-angle impact was essentially analyzed in Artemieva et al. (2004). As one can see from Table 1, a decrease in impact velocity leads to a decrease in impact melt production. However, the dependence is not

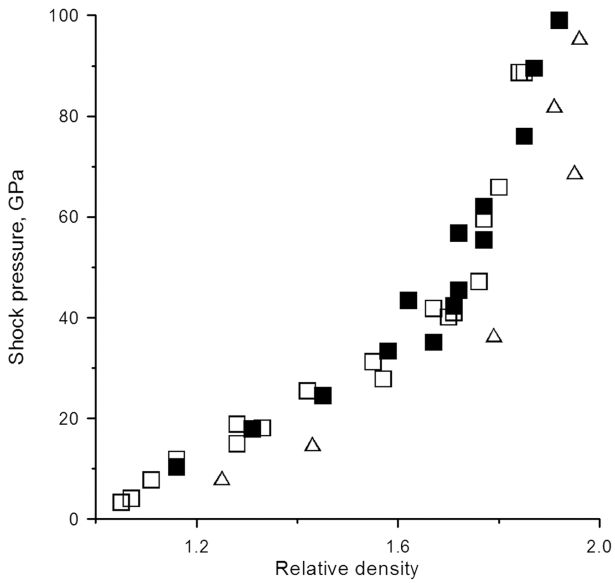

Fig. 3. Hugoniot curves for various silica-rich materials. Triangles = clay; open squares = silica; black squares = granite.

strong: it is easy to show that for a given crater size melt volume is approximately proportional to the cube root of impact velocity, i.e., melt volume at a velocity of 11.2 km/s (the lowest possible pre-atmospheric impact velocity on Earth) is only 20% lower than at an impact velocity of 18 km/s (the average impact velocity for the Earth). For the smallest craters on Earth (<3 km in diameter), final impact velocity may be substantially lower than pre-atmospheric velocity because of strong disruption and deceleration of the projectile in the atmosphere (Melosh and Collins 2005). This is a very special case in which a lot of projectile fragments and smaller craters (strewn field) can be identified near the crater rim (Artemieva and Bland 2003). Certainly, the Bosumtwi crater is not within this size range.

The influence of impact angle is not obvious, because the process of crater formation itself in a highly oblique impact is still uncertain. However, according to Table 1, even in the case where oblique impacts are as efficient as vertical ones, we should not expect the melt volume produced in an oblique impact to be more than a factor of 2–5 smaller than that formed in a vertical impact. An extreme decrease of impact melt production by a factor of 5 would still result in formation of a melt sheet tens of meters thick. This would also imply that the Bosumtwi impact was highly oblique (less than 30 degrees), which is inconsistent with models of tektite production (Artemieva 2002).

Specific Target Properties

The Bosumtwi Target Rocks

The crater was excavated in 2.1–2.2 Ga old metasediments and metavolcanics of the Birimian Supergroup (Koeberl et al. 1998). These rocks are primarily interbedded phyllites and mica-schists, meta-tuffs, meta-graywacke, quartzitic graywacke, shales, and slates. The porosity of undeformed (but probably subjected to weathering) samples collected from exposed road cuts near the crater was analyzed by Brown et al. (2006). Envelope densities of the rocks range from approximately 2.1 g/cm^3 to 2.4 g/cm^3 with corresponding porosities from 22% to 12%. Grain densities are consistent with the major minerals expected in metasediments. The porosity of 11 surface samples (phyllite graywacke, granite dikes, Pepiakese granite) measured by Plado et al. (2000) are lower and vary from 4.9 to 12.4 vol%. Although extrapolation from surface samples to a depth of a few kilometers is not reliable, porosity probably played an important role in crater formation. Also, taking into account the crater's location near the equator (06°30′N and 01°25′W) within the monsoon zone and hydrothermal alteration of target rocks (Karikari et al. 2007), wet porosity is quite probable.

Target Properties 1: Granite versus Other Silica-Rich Rocks

In our model we used granite as the main target material. Analysis of the LB-07A core (Coney et al. 2007) shows that granite, which is abundant in the fallout suevites, forms only a minor component of the fallback breccias and basement rocks. Although only a rather poor database of materials to be used in the models exists, sandstone could be a closer analogue than granite for the target rocks at Bosumtwi. However, Hugoniot curves for all silicate rocks are very similar (Fig. 3, based on experimental data from Trunin et al. 2001). Silica or silicate mineral glasses (single crystals or nonporous rocks) are formed by shock compression in the pressure range of about 25 to 55 GPa, whereas total rock fusion requires peak pressures in excess of 60–80 GPa (Stöffler 1984). Threshold pressures for melting modeled by ANEOS (Pierazzo et al. 1997) may differ somewhat from those of real materials, although they are in fact very close to experimentally based estimates. Certainly, this cannot explain substantial shock melt deficiency in the models.

Target Properties 2: Dry Porosity

Porosity influences crater formation and melt production in two ways. First, pressure decay in porous targets is much more abrupt than in solid materials because of the additional irreversible work needed to crush void space. Thus, a smaller crater and less highly shocked material is expected in a porous target for the same projectile size and velocity (Love et al. 1993; Wünnemann et al. 2005). On the other hand, porous rocks melt at lower shock pressures (Stöffler 1984). For example, in sandstone with 25% porosity melting could occur at pressures below 30 GPa. It is difficult to estimate both effects quantitatively, but it is highly unlikely that the net effect is sufficient to explain the complete absence of a coherent melt sheet. A preliminary study of impact cratering

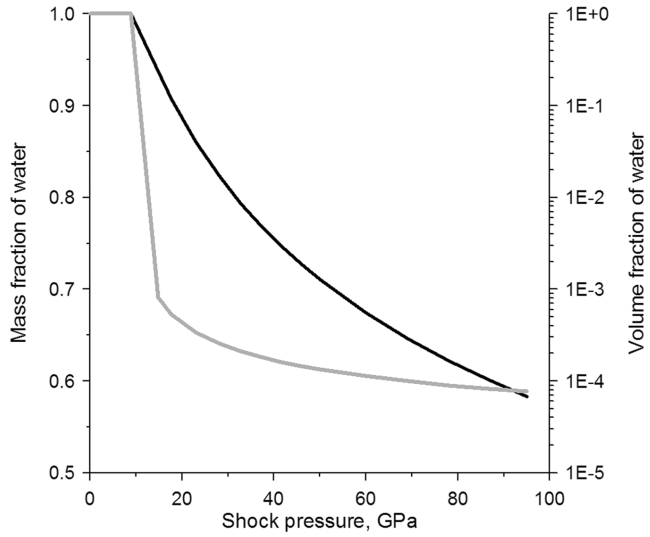

Fig. 4. Mass and volume fraction of liquid water after decompression from a given value of shock (for pure water). While the mass fraction is rather high (black curve and left axis), the two-phase mixture volume is totally defined by vapor (gray curve and right axis). In the case of 10% wet porosity, the final state of a silica-water mixture is also defined by water vapor; quartz particles and water droplets occupy a tiny fraction in the total mixture volume.

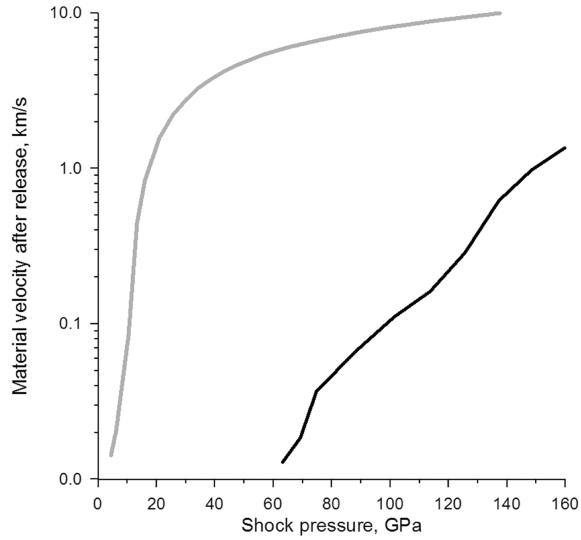

Fig. 5. Residual velocities after shock compression and release in pure water (gray line) and quartz (black line).

and melt production in porous targets (Wünnemann and Collins 2006) shows an increase of melt production with increasing porosity.

Target Properties 3: Wet Porosity or Other Volatiles

Melt and high-temperature solid ejecta modification by water and other volatiles in the target have been discussed quantitatively in Kieffer and Simonds (1980). They pointed out at least three sources of volatiles: vaporization of rocks themselves (at pressures above hundreds of GPa), decarbonation of limestones (P > 40–80 GPa), and vaporization of "free" water in pore spaces or on the surface (P > 10 GPa). In the case of the Bosumtwi event we can probably neglect the first and second effects, as vaporization of rocks is negligible and carbonates are not common for this target (although some carbonates occur in the cores) (Coney et al. 2007). Also we can neglect bound water in hydrous minerals. Free water could be significant, however.

Figure 4 shows mass and volume fraction of liquid water after adiabatic release from various shock pressures to standard atmospheric conditions, with the remainder being water vapor. The curves were constructed with the ANEOS equation of state for water and probably underestimate the amount of vapor. The important observation is that for moderate shock pressures, even though vaporization is not complete (less than 50% even at 100 GPa), the final state of the water-vapor mixture is dominated by the vapor; the volume fraction of the vapor is substantially greater than the volume of liquid droplets. It is easy to show that if the initial volume fraction of pore water in rocks is α (usually in the range of 0.05–0.20) and the ratio of water/vapor volume after release is δ (1000 after the release from 50 GPa) (see Fig. 4), then the vapor/(liquid+rocks) volume ratio is $\delta/(1 + 1/\alpha)$, i.e., 48–170. Also the excavation velocity within the crater (the residual of material velocities in the shock and the rarefaction wave after total decompression) is usually small, but dramatically increases if a phase transition occurs after decompression (Melosh, p. 42–43). Figure 5 shows residual velocities in water and in quartz calculated with the ANEOS package. Whilst the velocity in quartz does not exceed 100 m/s after decompression from 100 GPa, the velocity in water for the same compression is about 8 km/s. Silica materials with shock-metamorphic features typical for 30–40 GPa are characterized by negative residual velocities of tens of m/s (i.e., the material moves in the same direction as in the shock wave), while water vapor expands at 1–2 km/s. Thus, water vaporization after shock compression above 10–20 GPa may define the dynamics of the rock/melt/water mixture, and potentially eject much of the melted rock from the crater. The vapor could additionally disrupt the solid matrix, breaking it into smaller fragments, accelerate these fragments, and create a vapor cloud in which particles of different sizes and states of shock compression are mixed intensively.

The critical question is: how much water is required to have a substantial effect on crater excavation? Even a few volume percent of water in sandstone seemingly dramatically increase the final crater volume in high-velocity experiments (e.g., Kenkmann et al. 2006). For further insight, consider some useful examples that come from volcanology and technology. Natural steam explosions are common in terrestrial volcanoes where magma interacts with near-surface water (Colgate and Sigurgeirsson 1973, Wohletz and Sheridan 1983). Similar (but not identical) effects, known as "melt-coolant" (or fuel-coolant) interaction, occur in

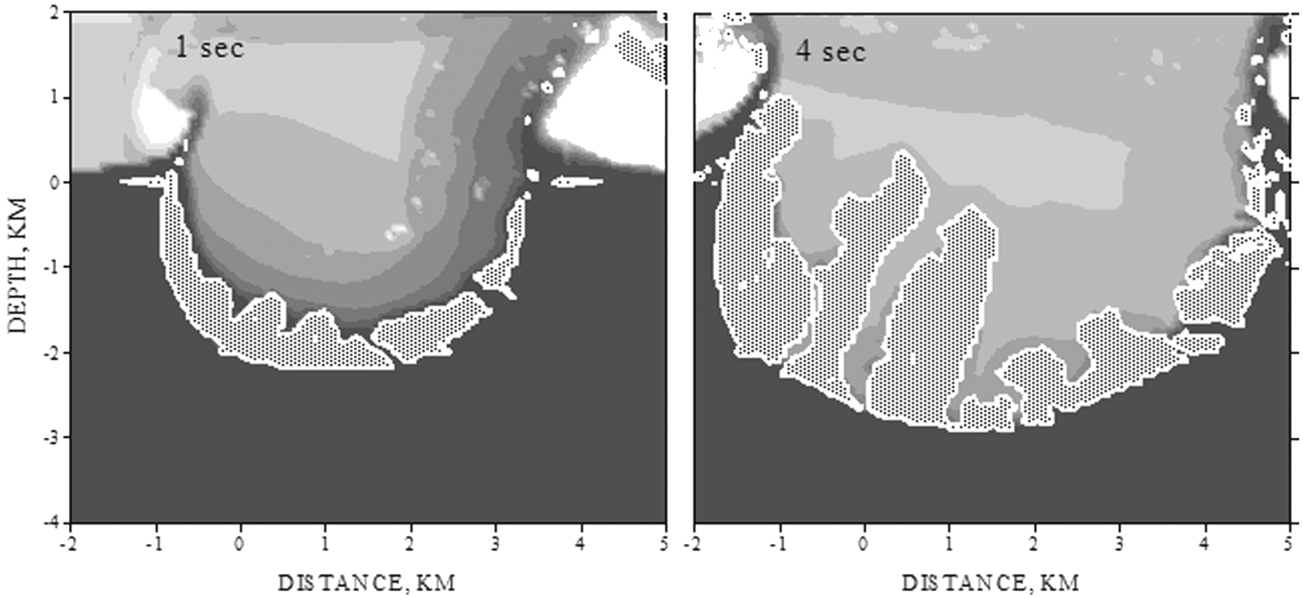

Fig. 6. Crater excavation in a mixed target with 10 vol% water after a 18 km/s impact at 45°. Water vapor is shown by dotted areas. At 1 s after the impact, water separation starts beneath the surface, where shock compression was high enough to vaporize water but not quartz. At 4 s after the impact, vaporized water is totally separated from the solid-molten quartz phase.

foundries and nuclear power plants. (Sandia Laboratories 1975). In these cases, explosion efficiency depends on the water-melt ratio and has a maximum (there is no explosion without water and explosive interaction is suppressed by a large amount of water). Experiments by Wohletz and Sheridan (1983) led to estimation of this maximum at 0.3–0.4, whereas a later study by Zielinsky (1995) gives much lower values of 0.03–0.04. Essentially, the efficiency of experimental explosions strongly depends on the degree of mixing and may differ by an order of magnitude. "Ideal" numerical modeling, assuming perfect melt-water mixture, gives a value of about 0.2 (Shuvalov and Artemieva 2004). Experiments with a water-melt mass ratio of about 0.2 (Wohletz and Sheridan 1983) revealed specific explosion characteristics and the interaction of ejected melt fragments with the expanding vapor cloud. Larger fragments follow ballistic parabolic paths, whereas small-sized ejecta experience significant aerodynamic drag due to their interaction with superheated steam. This critical value of 0.2 can be compared with potential water saturation at Bosumtwi. According to available data of rock porosity at the Lake Bosumtwi impact site (Plado et al. 2000; Brown et al. 2006) and assuming complete saturation, the water volume content might have been in the range from 5 to 20%, i.e., 4–10% by mass. This is close to, but less than the experimental and numerical values for maximum efficiency of "water-melt" explosion.

The main difference between a fuel-coolant system and volcano on the one hand, and a rock-pore-water system in an impact crater on the other, is that in the former case the water is initially cold and gains its energy from heat exchange with the magma, whereas in the latter case pore-water is superheated by shock wave propagation. Thus, the proportion between water and rocks to maximize an "explosion" may be different in impact cratering and in magma-water interaction. A comprehensive model of impact cratering in a water-saturated target should include, first, correct definition of the compression stage, including compression and pore compaction, and second, correct description of adiabatic expansion, in which rock fragmentation, water-vapor-solid separation, and their heat-momentum exchange, depending on the size-frequency distribution of fragments, occur. The rock-water impact system is certainly in mechanical equilibrium (i.e., both components have the same pressures), but probably not in total thermodynamic equilibrium (the temperature may be different, depending on the scale of the event in comparison with the scale of nonhomogeneity (Pierazzo et al. 2005). Fluids are likely to change the mode and yield of impact-induced failure in rocks (Ahrens and Rubin 1993). Also, the presence of target water may change the mode of impactite emplacement during cratering. While the final deposition and distribution of shocked materials within craters in dry crystalline targets is likely to be fairly laminar, due to interparticle cohesion and gravity, the behavior of rock-vapor mixture in water-rich targets could be much more turbulent, similar to dense turbulent pyroclastic flows (Artemieva 2006), in which vapor turbulence dominates.

As such a model is not available yet, in this paper I present two possible endmembers scenarios and contrast these models with the dry case. The first endmember model uses a standard (similar to Artemieva et al. 2004) impact

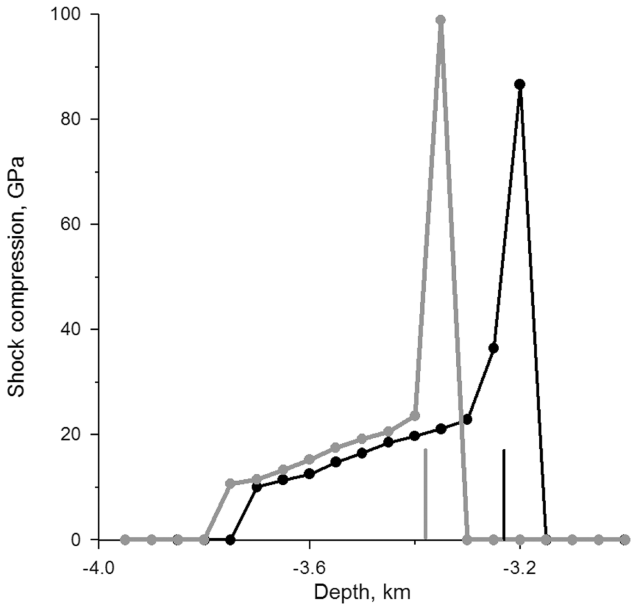

Fig. 7. Pressure distribution in "calculated" drill cores: gray curve for wet target, black curve for dry target. Vertical lines show the boundary between crater floor and vapor plume.

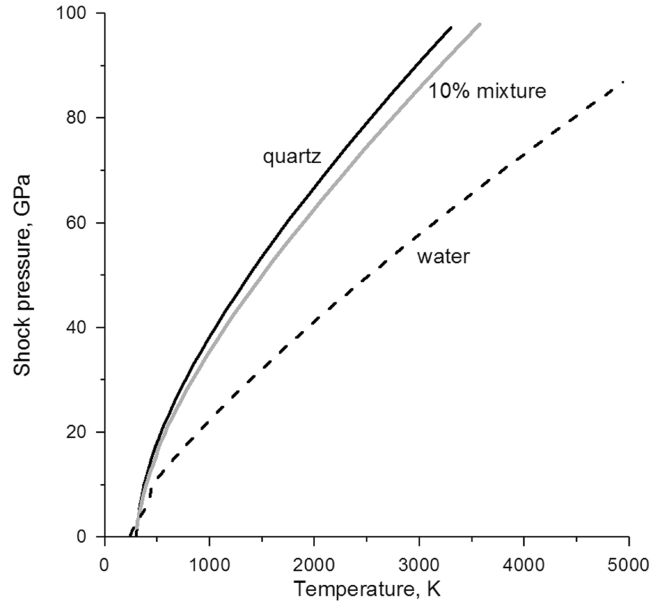

Fig. 8. Hugoniot of quartz (black solid line), water (black dashed line), and 10 vol% quartz-water mixture (gray line).

model, but into a target where each computational cell contains 10% (by volume) of water. The internal properties of the SOVA code tend to separate different materials and merge identical materials; hence, as water in highly compressed cells vaporizes and expands, clouds of merged water vapor form above the growing crater during the excavation stage (Fig. 6). In this case vapor-rock interaction is minimal, as materials are in mechanical equilibrium, but do not exchange heat. Also the model description of rocks as a continuum with rather low resolution (40 m cell size) does not allow intensive material mixing.

Pressure distributions with depth in the crater center at the end of the excavation stage are shown in Fig. 7, for this "wet" model and for a "dry" model in which no water was present in the target. In each case the peak pressures were found by averaging the maximum pressures recorded by tracers within a column of boxes 200 × 200 × 50 m (each box usually contains 10–40 tracers) located below the crater center. This column of boxes may be treated as a numerical analog of a real drill core. The vertical lines in Fig. 7 show the boundary between solid rocks and vapor (abrupt change in calculated density distribution)—thus the extremely high pressures correspond to material above the surface, not within the target rocks (pressure deviations recorded at this point are also extremely high, of the same order as maximum values). Even though pressures below 25 GPa show a similar distribution with depth in the dry and wet target, there are no pressures above this level in wet target. Although only two numerical cores are presented in the figure, the results of other "cores" look similar and an absence of highly compressed target rocks is systematic (the last recorded pressures in the target are 36-49-29 GPa in dry target and 23-27-22 GPa in wet target). Thus, the value of maximum shock compression in numerical wet "cores" is in agreement with observations in the LB-07A and the LB-08A cores (Coney et al. 2007; Deutsch et al. 2007; Ferrière et al. 2007).

The second endmember model that I considered assumes maximum water-rock interaction: I calculated Hugoniot and release curves assuming total mixing and total equilibrium (e.g., pressure and temperature) of both components. Physically, this case corresponds to rocks disrupted into tiny fragments that are in total equilibrium with vapor. As water content is rather low (the same 10 vol% as in the first example), the Hugoniot of the mixture follows the Hugoniot for quartz (Fig. 8) with a mixture temperature a bit higher (for the same shock pressure) than for pure quartz because of the presence of a low-impedance material (water). The release curves from 50 GPa and 30 GPa are shown in Fig. 9. The mixture density initially follows the same path as quartz density to the point where quartz reaches its normal density (at ~1100 K at the release from 50 GPa and at ~700 K at the release from 30 GPa). Then the water vapor continues to expand, the mixture density drops, and the water volume fraction increases sharply. Soon after this point, the procedure of pressure equalization for the two components failed. Physically, this means that beyond this point quartz cannot be treated as a continuum and the water vapor must be considered to be mixed with solid fragments (i.e., the mixture pressure is defined by the vapor alone, while the internal energy is the sum of vapor and particles energy). However, at this point the material velocity in the rarefaction wave has practically reached its final value of 3 and 2 km/s (for compression to 50 and 30 GPa, respectively), as the sound

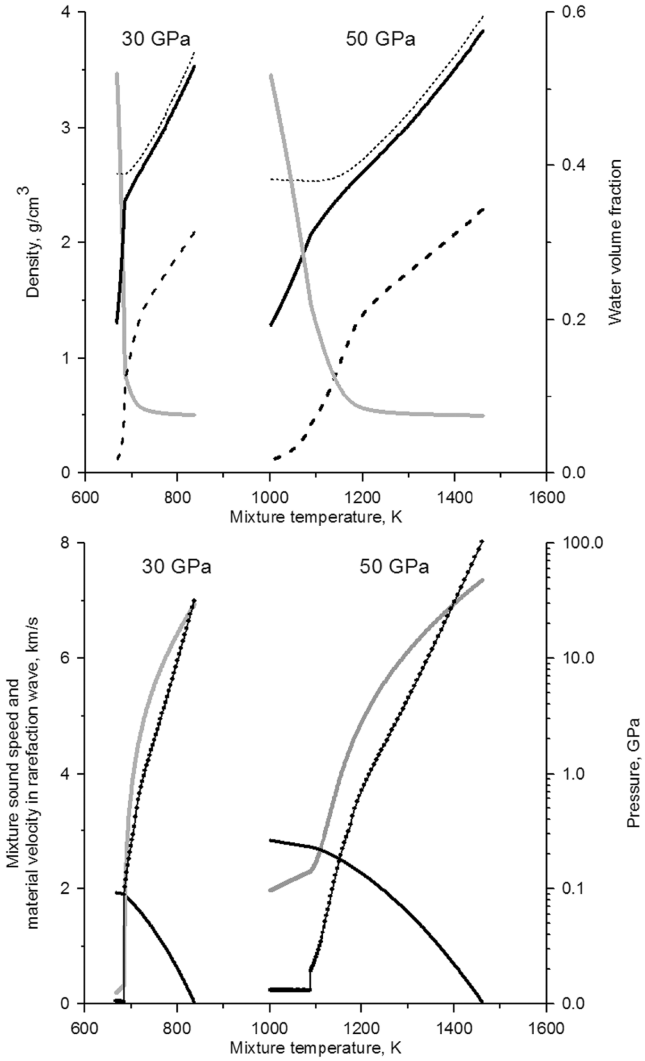

Fig. 9. Release curves for the mixture compressed to 30 and 50 GPa. Upper plate, left axis: mixture density (solid line) and densities of quartz (dotted line) and water (dashed line) as a function of temperature. Upper plate, right axis: volume water content. Bottom plate, left axis: sound speed in the mixture (dotted line) and material velocity in the rarefaction wave (black solid line). Bottom plate, right axis: pressure as a function of temperature.

speed is extremely low in the two-phase region (see Fig. 9, bottom plate). The values of residual material velocities are 0.22 and 0.05 km/s (and less than 10 m/s after release from 10 GPa). These values are substantially less than residual velocities in pure water (4.8, 2.7, and 0.08 km/s), but appreciably higher than in quartz (negative values, all below 10 m/s). Roughly, in this pressure range the mixture residual velocities can be estimated as water residual velocities multiplied by water mass fraction of 0.04. This analysis suggests that, even assuming a low water content, the velocities in a vapor-rock mixture are high enough to allow ejection of the heavy vapor plume from the crater or at least substantial redistribution of shocked minerals.

In both endmember models, which assume little or complete mixing of rock and water vapor, during vapor plume expansion, the presence of water does not change the degree of shock compression of geological materials, or their final physical state (solid-melt-vapor), but it does substantially modify the process of final material distribution, with highly compressed fractions being intensively dispersed. It is extremely difficult to reproduce this effect in laboratory experiments, as the highest shock compression is usually achieved in a confined container (e.g., Deutsch et al. 2007), whereas expansion of the vapor-rock mixture is of crucial importance.

CONCLUSIONS AND UNRESOLVED PROBLEMS

Numerical and geophysical models of the Bosumtwi crater suggest the presence of a coherent melt sheet and a monotonic decrease in shock metamorphism with depth. Analysis of two drill cores into the crater shows that no coherent melt is present and that impactites that experienced varying degrees of shock are well mixed. It is unlikely that the absence of coherent melt is due to either inaccurate characterization of the target, low velocity impact, or low angle impact. If these two drill cores provide representative samples of the crater fill and crater floor, the dramatic discrepancy between the predictions of numerical and geophysical modeling and results from the Bosumtwi core data is most probably due to turbulent dispersion of impactites driven by the vaporization of water in the target, although other volatiles may have played a similar role. This requires that the target rocks at Bosumtwi had at least 10 vol% water to a depth of several km. This number does not contradict available geological data for the samples collected near the Lake Bosumtwi. Also, observations of decorated PDFs in Bosumtwi samples (Ferrière 2007) argue for an impact into a water-bearing target. This might be evidence that solid-vapor interaction defines ejecta distribution in terrestrial craters within sedimentary targets or targets with high water content, as it does certainly in volcanic eruptions. This also has implications for ejection processes on Mars (e.g., Barlow et al. 2006).

The successful Bosumtwi crater drilling project provides crucial data for the development of more sophisticated numerical models. Future modeling should concentrate on quantifying the role of porosity, both wet and dry, on the production and dispersion of melt during an impact. This should be accompanied by geologic investigation of the actual pre-impact porosity and water content in local target materials, and a search for evidence of rock-water interaction and the distribution of solid and molten fragments with distance from the crater.

Acknowledgments–Drilling at Bosumtwi was supported by the International Continental Scientific Drilling Program

(ICDP), the U.S. NSF-Earth System History Program under grant no. ATM-0402010, Austrian FWF (project P17194-N10), the Austrian Academy of Sciences, and by the Canadian NSERC. Drilling operations were performed by DOSECC. The author was supported by the Russian Foundation of Basic Research (grant 04-05-64209) and by the NASA PG&G Program (grant NNX06AD75G). I highly appreciate valuable reviews by Gareth Collins (who also provided linguistic editing) and Kai Wünnemann. Many thanks for permanent support and friendly criticism from my colleagues A. Deutsch, B. Ivanov, C. Koeberl, B. Milkereit, and U. Reimold.

Editorial Handling—Dr. Christian Koeberl

REFERENCES

Ahrens T. J. and O'Keefe J. D. 1972. Shock melting and vaporization of lunar rocks and minerals. *Moon* 4:214–249.

Ahrens T. J. and O'Keefe J. D. 1977. Equations of state and impact-induced shock-wave attenuation on the Moon. In *Impact and explosion cratering*, edited by Roddy D. J., Pepin R. O., and Merrill R. B. Elmsford, New York: Pergamon Press. pp. 639–656.

Amsden A. A., Ruppel H. M., and Hirt C. W. 1980. SALE, A Simplified ALE computer program for fluid flow at all speeds. Los Alamos National Laboratories Report #LA-8095. Los Alamos, New Mexico. 101 p.

Artemieva N. A. 2002. Tektite origin in oblique impact: Numerical modelling. In *Impacts in Precambrian shields*, edited by Plado J. and Pesonen L. Berlin: Springer Verlag. pp. 257–276.

Artemieva N. 2006. Fluidized impact ejecta and volcanic blast surge—Numerical modeling (abstract #1525). 37th Lunar and Planetary Science Conference. CD-ROM.

Artemieva N. and Bland P. 2003. Crater fields on Venus, Earth, and Mars (abstract #1319). 34th Lunar and Planetary Science Conference. CD-ROM.

Artemieva N., Karp T., Milkereit B. 2004. Investigating the Lake Bosumtwi impact structure: Insight from numerical modeling. *Geochemistry Geophysics Geosystems* 5, doi:10.1029/2004GC000733.

Barlow N. G., Stewart S., and Barnouin-Jha O. S. 2006. Proceedings of the Workshop on the Role of Volatiles and Atmospheres on Martian Impact Craters. *Meteoritics & Planetary Science* 41: 1423–1424.

Brown M., Schmitt D. R., Milkereit B., Claeys P. 2006. Porosity in impact damaged rocks: Inferences from scientific drilling in the Lake Bosumtwi, Ghana, impact structure. (abstract #1507). 37th Lunar and Planetary Science Conference. CD-ROM.

Chapman C. R. and McKinnon W. B. 1986. Cratering of planetary satellites. In *Satellites*, edited by Burns J. and Matthews M. S. Tucson, Arizona: The University of Arizona Press. pp. 492–580.

Colgate S. A. and Sigurgeirsson R. 1973. Dynamic mixing of water and lava. *Nature* 244:552–555.

Coney L., Gibson R. L., Reimold W. U., and Koeberl C. 2007. Lithostratigraphic and petrographic analysis of ICDP drill core LB-07A, Bosumtwi impact structure, Ghana. *Meteoritics & Planetary Science* 42. This issue.

Deutsch A., Heinrich V., and Luetke S. 2006. The Lake Bosumtwi Impact Crater Drilling Project (BCDP): Lithological profile of wellhole BCDP-8A (abstract #1292). 37th Lunar and Planetary Science Conference. CD-ROM.

Deutsch A., Luetke S., and Heinrich V. 2007. The ICDP Lake Bosumtwi impact crater scientific drilling project (Ghana): Core LB-08A litho-log, related ejecta, and shock recovery experiments. *Meteoritics & Planetary Science* 42. This issue.

Ferrière L., Koeberl C., and Reimold W. U. 2007. Drill core LB-08A, Bosumtwi impact structure, Ghana: Petrographic and shock metamorphic studies of material from the central uplift. *Meteoritics & Planetary Science* 42. This issue.

Glass B. P., Kent D. V., Schneider D. A., and Tauxe L. 1991. Ivory Coast microtektite strewn field: Description and relation to the Jaramillo geomagnetic event. *Earth and Planetary Science Letters* 107:182–196.

Grieve R. A. F. and Cintala M. J. 1992. An analysis of differential impact melt-crater scaling and implications for the terrestrial impact record. *Meteoritics* 27:526–538.

Grieve R. A. F. and Pesonen L. L. 1992. The terrestrial impact cratering records. *Tectonophysics* 216:1–30.

Grieve R. A. F. and Robertson P. B. 1979. The terrestrial cratering records, 1: Current status of observations. *Icarus* 38:212–229.

Grieve R. A. F., Dence M. R., and Robertson P. B. 1977. Cratering processes: As interpreted from the occurrence of impact melts. In *Impact and explosion cratering*, edited by Roddy D. J., Pepin R. O., and Merrill R. B. New York: Pergamon Press. pp.791–814.

Grieve R. A. F., Reny G., Gurov E. P., and Ryabenko V. A. 1987. The melt rocks from the Boltysh impact crater, Ukraine, USSR. *Contributions to Mineralogy and Petrology* 96:56–62.

Gurov E. P. and Gurova E. P. 1985. Boltysh astrobleme: Impact crater pattern with a central uplift (abstract). 16th Lunar and Planetary Science Conference. pp. 310–311.

Ivanov B. A. 2002. Deep drilling results and numerical modeling: Puchezh-Katunki impact structure, Russia (abstract #1286) 33rd Lunar and Planetary Science Conference. CD-ROM.

Ivanov B. A. and Artemieva N. A. 2002. Numerical modeling of the formation of large impact craters. In *Catastrophic events and mass extinctions: Impact and beyond*, edited by Koeberl C. and MacLeod K. G. GSA Special Paper #356. Boulder, Colorado: Geological Society of America. pp. 619–630.

Karikari F., Ferrière L., Koeberl C., Reimold W. U., and Mader D. 2007. Petrography, geochemistry, and alteration of country rocks from the Bosumtwi impact structure, Ghana. *Meteoritics & Planetary Science* 42. This issue.

Karp T., Milkereit B., Janle P., Danuor S. K., Pohl J., Berckhemer H., and Scholz C. A. 2002. Seismic investigation of the Lake Bosumtwi impact crater: Preliminary results. *Planetary and Space Science* 50:735–743.

Kenkmann T., Thoma K., Deutsch A. and the MEMIN Team. 2006. Hypervelocity impact into dry and wet sandstone (abstract #1587). 37th Lunar and Planetary Science Conference. CD-ROM.

Kieffer S. W. and Simonds C. H. 1980. The role of volatiles and lithology in the impact cratering process. *Reviews of Geophysics and Space Physics* 18:143–181.

Koeberl C., Reimold W. U., Blum J. D., and Chamberlain C. P. 1998. Petrology and geochemistry rocks from the Bosumtwi impact structure, Ghana, and comparison with Ivory Coast tektites. *Geochimica et Cosmochimica Acta* 62:2179–2196.

Koeberl C., Milkereit B., Overpeck J. T., Scholz C. A., Peck J., and King J. 2005. The 2004 ICDP Bosumtwi impact crater, Ghana, West Africa, drilling project: A first report (abstract #1830). 36th Lunar and Planetary Science Conference. CD-ROM.

Love S. G., Hörz F., and Brownlee D. E. 1993. Target porosity effects in impact cratering and collisional disruption. *Icarus* 105:216–224.

Masaitis V. L. 1992. *Impactites from Popigai crater.* International Conference on Large Meteorite Impacts and Planetary Evolution.

August 31–September 2, 2002, Ontario, Canada. LPI Contribution #790. Houston, Texas: Lunar and Planetary Institute. p. 51.

Masaitis V. L. 1998. Popigai crater: Origin and distribution of diamond-bearing impactites. *Meteoritics & Planetary Science* 33:349–359.

Melosh H. J. 1989. *Impact cratering: A geological process*. New York: Oxford University Press. 245 p.

Melosh H. J. and Collins G. S. 2005. Meteor Crater formed by low-velocity impact. *Nature* 434:157.

Morrow J. 2007. Shock-metamorphic petrography and microRaman spectroscopy of quartz in upper impactite interval, ICDP drill core LB-07A, Bosumtwi impact crater, Ghana. *Meteoritics & Planetary Science* 42. This issue.

Pesonen L. J., Koeberl C., Ojamo H., Hautaniemi H., Elo S., and Plado J. 1998. Aerogeophysical studies of the Bosumtwi impact structure, Ghana. *GSA Abstracts with Programs* 30:A-190.

Pevzner L. A., Kirjakov A. F., Vorontsov A. K., Masaitis V. L., Mashchak M. S., and Ivanov B. A., 1992. Vorotilovskaya drill hole: First deep drilling in the central uplift of large terrestrial impact crater (abstract). 23rd Lunar and Planetary Science Conference. pp. 1063–1064.

Pierazzo E. and Melosh H. J. 2000. Melt production in oblique impacts. *Icarus* 145:252–261.

Pierazzo E., Vickery A., and Melosh H. J. 1997. Re-evaluation of impact melt production. *Icarus* 127:408–423.

Pierazzo E., Artemieva N., and Ivanov B. 2005. Starting conditions for hydrothermal systems underneath Martian craters: Numerical modeling. In *Large meteorite impacts III*, edited by Kenkmann T., Hörz F., and Deutsch A. GSA Special Paper #384. Boulder, Colorado: Geological Society of America. pp. 443–457.

Plado J., Personen L. J., Koeberl C., and Elo S. 2000. The Bosumtwi meteorite impact structure, Ghana: A magnetic model. *Meteoritics & Planetary Science* 35:723–732.

Pohl J., Stöffler D., Gall H., and Ernston K. 1977. The Ries impact structure. In *Impact and explosion cratering*, edited by Roddy D. J., Pepin R. O., and Merrill R. B. New York: Pergamon Press. pp. 343–404.

Reimold W. U., Coney L., Koeberl C., and Gibson R. L. 2006. ICDP borehole LB-07A (Bosumtwi impact structure, Ghana): An overview and first multidisciplinary results (abstract #1350). 37th Lunar and Planetary Science Conference. CD-ROM.

Sandia National Laboratories. 1975. Core-meltdown experimental review. SAND-74-0382. New Mexico: Sandia National Laboratories.

Scholz C. A., Karp T., Brooks K., Milkereit B., Amoako P. Y. O., and Arko J. A. 2002. Pronounced central uplift identified in the Bosumtwi impact structure, Ghana, using multichannel seismic reflection data. *Geology* 30:939–942.

Shuvalov V. and Artemieva N. 2004. Numerical modeling of phreatomagmatic explosions. 26th Nordic Geological Winter Meeting. January 6–9, 2004, Uppsala, Sweden. *GFF* 126:50.

Shuvalov V. V., Artemieva N. A., and Kosarev I. B. 1999. 3-D hydrodynamic code SOVA for multimaterial flows, application to Shoemaker-Levy 9 comet impact problem. *International Journal of Impact Engineering* 23:847–858.

Simonds C. H. and Kieffer S. W. 1993. Impact and volcanism: A momentum scaling law for erosion. *Journal of Geophysical Research* 98:14,321–14,337.

Stöffler D. 1984. Glasses formed by hypervelocity impact. *Journal of Non-Crystalline Solids* 67:465–502.

Stöffler D., Artemieva N., Ivanov B., Hecht L., Kenkmann Th., Schmitt R. T., Tagle R. A., and Wittman A. 2004. *Meteoritics & Planetary Science* 39:1035–1067.

Trunin R. F., Gudarenko L. F., Zhernokletov M. V., and Simakov G. V. 2001. Experimental data on shock compression and adiabatic expansion of condensed matter. Russian Federal Nuclear Center RFNC-VNIIEF, Sarov. 446 p.

Wohletz K. H. and Sheridan M. F. 1983. Martian rampart crater ejecta: experiments and analysis of melt-water interaction. *Icarus* 56:15–37.

Wünnemann K.,Collins G. S., and Melosh H. J. 2005. A strain-based porosity model for use in hydrocode simulations of impacts and implications for transient crater growth in porous targets. *Icarus* 180:514–527.

Wünnemann K. and Collins G. S. 2006. The effect of porosity on meteorite impact process (abstract #EGU06-A-03991). *Geophysical Research Abstracts* 8.

Zel'dovich Ya. B. and Raizer Yu. P. 2002. *Physics of shock waves and high-temperature hydrodynamic phenomena.* Mineola, New York: Dover Publications. 916 p.